ADVANCES IN ATMOSPHERIC SCIENCES, VOL. 25, NO. 5, 2008, 765–777

Snowstorm over the Southwestern Coast of the Korean Peninsula Associated with the Development of Mesocyclone over the Yellow Sea

Ki-Young HEO and Kyung-Ja HA*

Division of Earth Environmental System, College of Natural Sciences, Pusan National University, Korea

(Received 2 March 2007; revised 26 February 2008)

ABSTRACT

This study investigates the characteristics of a heavy snowfall event over the southwestern part of the Korean Peninsula on 4 December 2005. The snowstorm was a type of mesoscale maritime cyclone which resulted from barotropic instability, and diabatic heating from the warm ocean in continental polar air masses.

Based on surface observations, radiosonde soundings, MTSAT-1R satellite data and the 10-km grid RDAPS (Regional Assimilation and Prediction System based on the PSU/NCAR MM5) data, the evolution of the mesocyclone is explained by the following dynamics; (1) In the initial stage, the primary role in the cyclogenesis process of the mesocyclone is a barotropic instability in the horizontal shear zone. (2) In the developing stage, the mesocyclone moves and deepens into a baroclinic zone corresponding to the surface heating and moistening. (3) In the mature stage, it is found that the mesocyclone is intensified by the destabilization caused by enhanced low-level heating and condensation, the moisture flux convergence, and the interaction between upper and lower-level potential vorticity anomalies.

We suggest that a checklist with stepwise indicators responsible for development be prepared for the forecasting of heavy snowfall over the southwestern part of the Korean Peninsula.

Key words: heavy snowfall, mesocyclone, baroclinic instability, barotropic instability, stepwise roles, potential vorticity anomalies

Citation: Heo, K. Y., and K. J. Ha, 2008: Snowstorm over the southwestern coast of the Korean Peninsula associated with the development of mesocyclone over the Yellow Sea. *Adv. Atmos. Sci.*, **25**(5), 765–777, doi: 10.1007/s00376-008-0765-2.

1. Introduction

In winter, the Korean Peninsula is often hit by massive snowfalls. Cho et al. (2004) mentioned the importance of low-level wind in snowfall incidents and suggested several checkpoints for improving the accuracy of snowfall forecasts. Heo et al. (2005) also showed that synoptic scale effects along with Conditional Symmetric Instability (CSI) considerably affected the formation of snowstorms in the southeastern part of the Korea. Seo and Jhun (1991) found that sensible heat flux and latent heat flux greatly affected the formation of marine lows. Yih and Walsh (1991) showed that the vertical velocities and precipitation rates were dependent on the ocean temperature perturbations in the case of extreme cyclone events. Xu and Zhou (1999) found that the explosive cyclogenesis occurred over wide spans of warm sea surface where strong baroclinicity and the low-level jet (LLJ) were initially formed under the favorable atmospheric circulation.

The Korean Peninsula, with its complicated geography, is surrounded by the sea on three sides (see Fig. 1). Usually, massive snowfalls over the western coast, including the Jeollanam-do, Jeollabuk-do, Chungcheongnam-do and Chungcheongbuk-do, are caused by the transformation of the winter monsoon air-mass from the Eurasian continent. Generally, these kinds of snowfalls are most frequent in December. However, research on heavy snowfalls is still insufficient.

A mesocyclone developed over the Yellow Sea inducing a heavy snowfall along the southwestern coast

*Corresponding author: Kyung-Ja HA, kjha@pusan.ac.kr

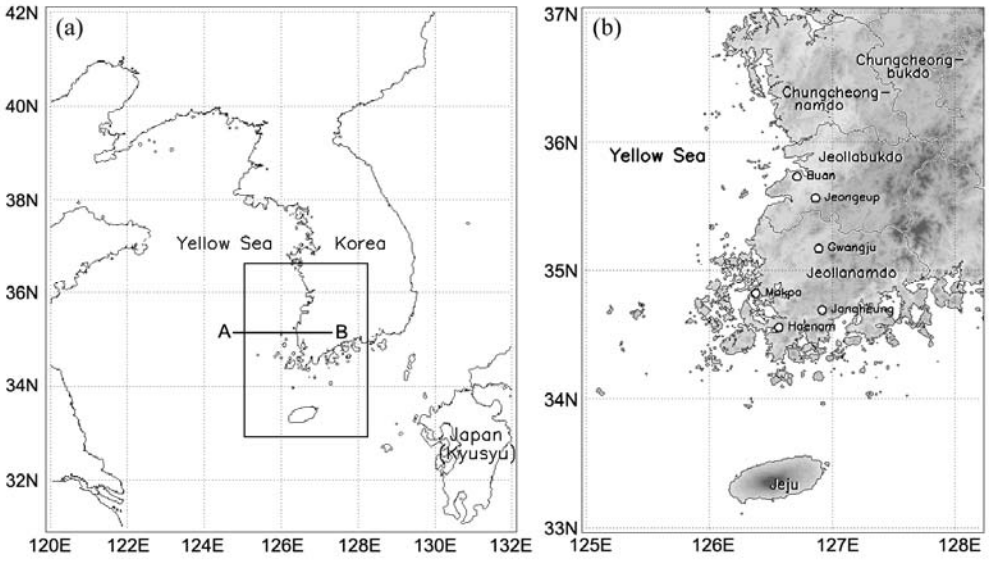

Fig. 1. Geographic maps of East Asia and the southwestern part of the Korean Peninsula. (a) Some observation stations referred to in the text are presented. The line AB indicates cross-section analysis which will be shown in Fig. 14. (b) Zoomed in map of Korean Peninsula.

of the Korean Peninsula on 4 December 2005. Snowfall began on the afternoon of 3 December in the middle part of Korea and on 4 December it expanded to cover the western coast. On 4 December, Jangheung, Haenam, Mokpo, and Jeongeup reported over 30 cm of snow per day, and most of Jeollanam-do and Jeollabuk-do reported over 20 cm (see Fig. 2). A snowfall amount above 20 cm was recorded over the western coast of Korea (hereafter named as western coast). Occasionally, winter snowfalls in the Korean Peninsula are caused by the development of marine low in the Yellow Sea. This kind of snowfall is usually concentrated in the southwestern coastal region.

This paper aims to investigate the cause of the record-breaking snowfall on 4 December 2005 over the southwestern coast of the Korean Peninsula. We will suggests a checklist for the forecasting of the mesocyclone other than the pre-existent one that was developed for heavy snowfall forecast in the southwestern part of Korea. We also will analyze the mesocyclogenesis and will document its structure. The rest of the present paper is organized in the following way. Section 2 will introduce the data used in the present study. Section 3 illustrates the large-scale environment

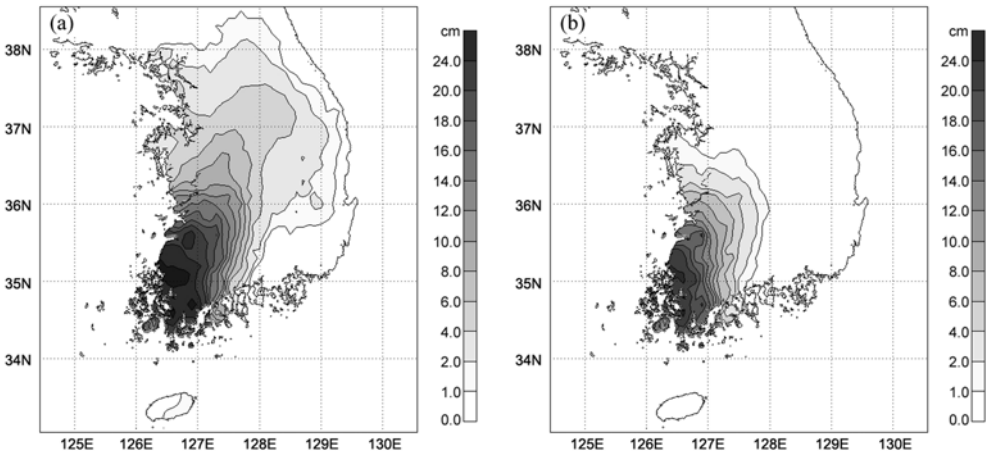

Fig. 2. Accumulated snowfall amount over the Korean Peninsula (units: cm). (a) from 1500 UTC 3 to 1500 UTC 4 December 2005. (b) from 0000 UTC to 0900 UTC 4 December 2005 based upon KMA data.

Table 1. Configuration of RDAPS high-resolution model (10 km).

Dynamics	Horizontal resolution	Vertical resolution	Forecast times	Initialization
Non-hydrostatic	10 km	33 levels/50 hPa	24 h	1-way interaction
Explicit scheme	Cumulus scheme	PBL scheme	Radiation scheme	Soil scheme
Mixed-phase	Kain-Fritach	MRF	Cloud Radiation	5-layer Soil
(Reisner et al., 1998)	(Kain and Fritsch, 1993)	(Hong and Pan, 1996)	(Dudhia, 1989)	(Dudhia, 1996)

associated with subsequent mesocyclone development. Section 4 describes the processes believed to play a critical role in producing the extensive snowband and destabilizing the atmosphere for the present storm. Finally, section 5 summarizes the results that highlight the major processes acting in the storm.

2. Data

The following data are employed in the present study. (1) Snowfall measurements at 76 stations on 4 December 2005; (2) Surface weather charts and upper weather charts; (3) Radiosonde data over Gwangju station (35.1°N, 126.8°E)[a]; (4) MTSAT (Multifunctional Transport Satellite)-1R satellite imagery from 0000 UTC to 0600 UTC 4 December 2005 (with 3-h interval) downloaded from the satellite information service system2 of KMA (Korean Meteorological Administration).

For detailed analysis, The RDAPS (Regional Data Assimilation and Prediction System) model data was used. The RDAPS based on the PSU/NCAR MM5 version 3 model, the KMA's regional forecast model, was run as the operational model twice a day (0000 and 1200 UTC) and was analyzed by 3-D optimal interpolation. Table 1 shows the configuration of the RDAPS. In this study, we used the output of a high-resolution model with a horizontal grid resolution of 10 km.

3. Large scale environment

The large scale environments are shown in Fig. 3, which represents 500 and 850 hPa charts and the surface chart at 0000 UTC and 0600 UTC 4 December 2005, respectively. At 500 hPa at 0000 UTC 4 (Fig. 3a), a cold cut-off vortex (−38°C) exists in the north part of the Korean Peninsula around 40°N, 125°E. Correspondingly, a synoptic scale trough is located over the Yellow Sea. The cut-off vortex at 500 hPa moves eastward and becomes more symmetric by 0600 UTC 4 (Fig. 3b). The approach of the upper-level cold vortex is a typical synoptic environment for an intense cyclogenesis including the polar low (Fu et al., 2004). Therefore, the existence of a deep trough in the NNE-SSW direction in the north part of Korea acts as a synoptic condition for the formation of a mesocyclone (Fig. 3a). The intensification of the low-level circulation is triggered by a 500 hPa cold vortex. At 850 hPa, the isotherms and isobars over the eastern coast of the China are almost perpendicular with each other, suggesting that the baroclinicity in that area is stronger (Figs. 3c and 3d). This synoptic condition, associated with subsequent mesocyclone development, is quite similar to the situation described by Lee et al. (1998). At the surface at 0000 UTC (Fig. 3e), a mesoscale low is located in the East Sea (the Sea of Japan) after passing the Korean Peninsula. During the next 6h, this mesoscale low deepens from 1008 hPa to 1000 hPa quickly, but its location is almost the same. Correspondingly, the southwestern coast of the Korean Peninsula is under the control of northerly winds.

4. Synoptic and mesoscale ana lyses

4.1 *Observational analysis*

Figure 4 shows MTSAT-1R visible imagery from 0033 UTC to 0633 UTC 4 December 2005. It is seen that a mesocyclone with organized convective clouds is evident over the southwestern coast of the Korean Peninsula at 0033 UTC 4 December 2005 (Fig. 4a). The MTSAT-1R imagery is useful for the analysis of evolution and movement of the mesocyclone. A wide distribution of convective clouds can be detected over the Yellow Sea. Furthermore, a convective cloud around (36°N, 124°E) (C1 in the following) to the northwest of mesocyclone and a relatively large convective cloud over the western coast around 35°N, 126°E (C2 in the following) imply that elongated low-level convergences are developed in those regions (Figs. 4a and b). Figure 4 shows the development process through the merging of eastward-moving C1 with stagnant C2. At 0033 UTC 4 December, C1 and C2 can be seen with a weak vortex in Fig. 4a. The C1 moves to the southeast while C2 is stagnant at 0300 UTC 4 December (Fig. 4b). A mesocyclone is finally devel-

[a]From http://weather.uwyo.edu/upperair/sounding.html

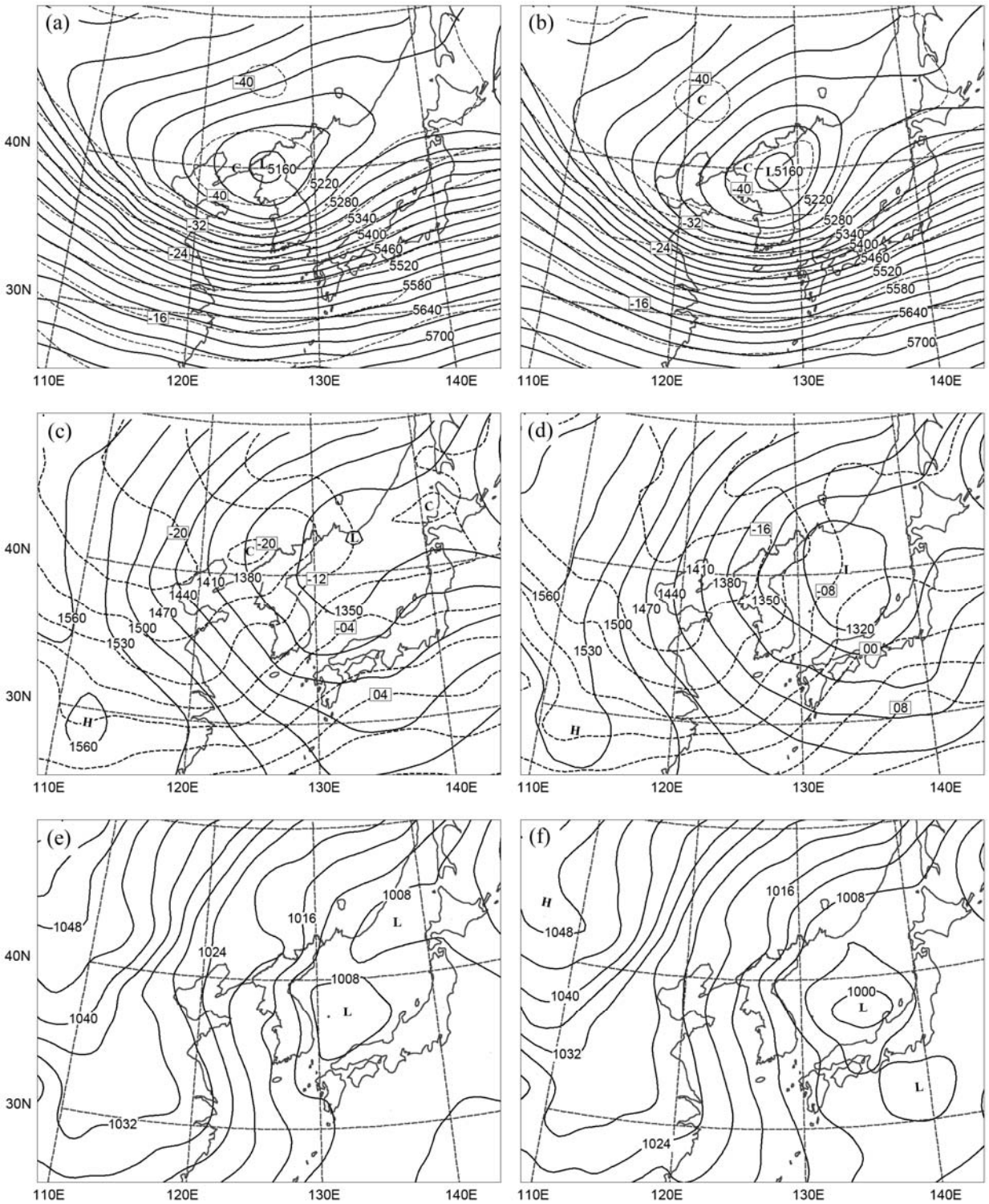

Fig. 3. Synoptic 500 hPa weather chart at (a) 0000 UTC. (b) 0600 UTC 4 December 2005. (c) and (d) are the same as (a) and (b), respectively, except for synoptic 850 hPa weather chart. (e) and (f) are the same as (a) and (b), respectively, except for surface weather chart. The solid lines represent the height contours [in (a), (b), (c) and (d), 30-gpm interval] or the isobars [in (e) and (f), 4 hPa interval]. The dashed lines represent the isotherms [in (a), (b), (c) and (d), 4°C interval].

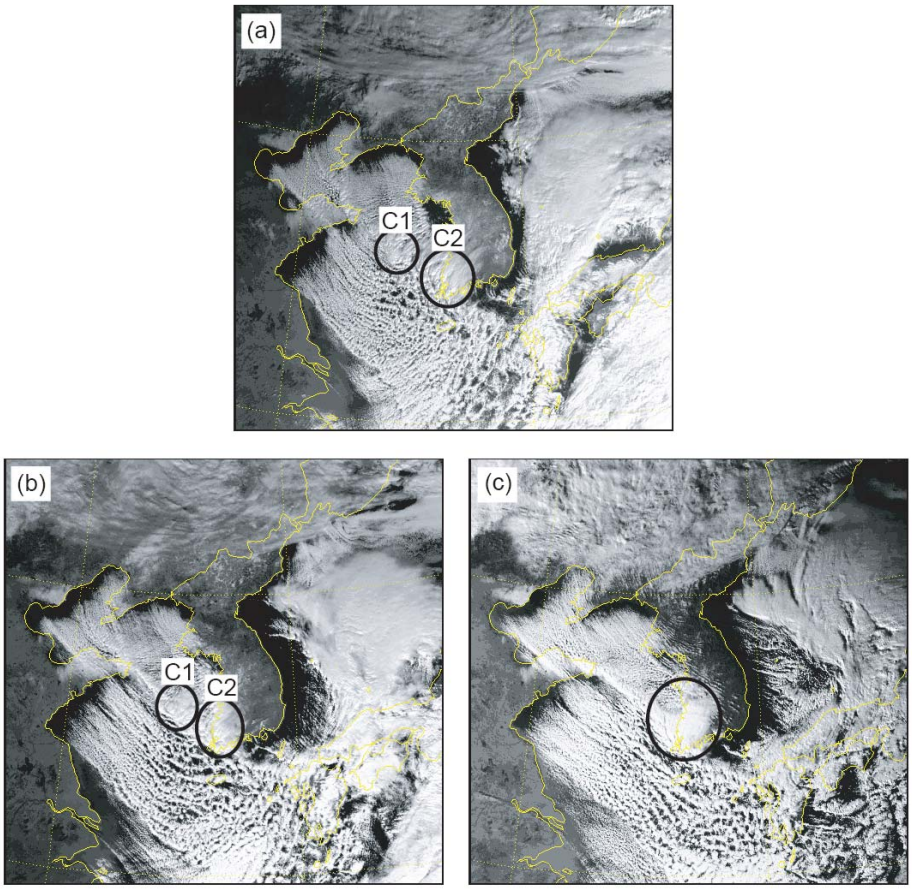

Fig. 4. MTSAT-1R visible satellite imagery. (a) 0033 UTC, (b) 0300 UTC, (c) 0633 UTC 4 December 2005. C1 and C2 indicate southeastward-moving convective cloud and stagnant convective cloud, respectively. A mesocyclone is developed by the merging of C2 with C1.

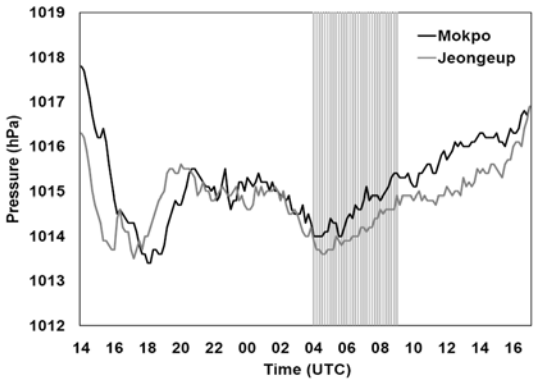

Fig. 5. Time series of the surface observations at (a) Mokpo and Jeongeup from 1400 UTC 3 December 2005 to 17 UTC 4 December 2005. The locations of the stations are indicated in Fig. 1. Shaded area indicates the massive snowfall above 3 cm h^{-1}.

oped when C2 with C1 merge at 0600 UTC 4 December (Fig. 4c). A well-developed mesocyclone is over the shear zone shown in Fig. 6.

The existence of these mesocyclones can be clearly seen in the time series of sea level pressure analyzed from AWS (Automatic Weather System) data (Fig. 5). The shaded area represents the time period with more than 3 cm h^{-1} of snowfall. After the passage of the synoptic low at 1700–1800 UTC 3 December, the pressure drops from 0000 UTC 4 December, reaching its minimum in 0400 UTC. The heavy snowfall occurred after the passage of the mesoscale low during the period from 0400 UTC to 0900 UTC 4 December. Heavy snowfall accompanies the fall of pressure, and 15.4 cm and 12 cm of snow is recorded in Buan and Jeongeup at 0300–0500 UTC. It is also found that SST is 15°C–18°C over the Yellow Sea, which exceed 4°C–5°C compared to the climatological SST (not shown).

4.2 *Analyses based upon numerical modeling*

The 10-km grid RDAPS model data is used for detailed analysis. Figure 6 shows the horizontal wind vector superimposed over the vorticity field at the lowest level (50 m) simulated by RDAPS from 0000 to

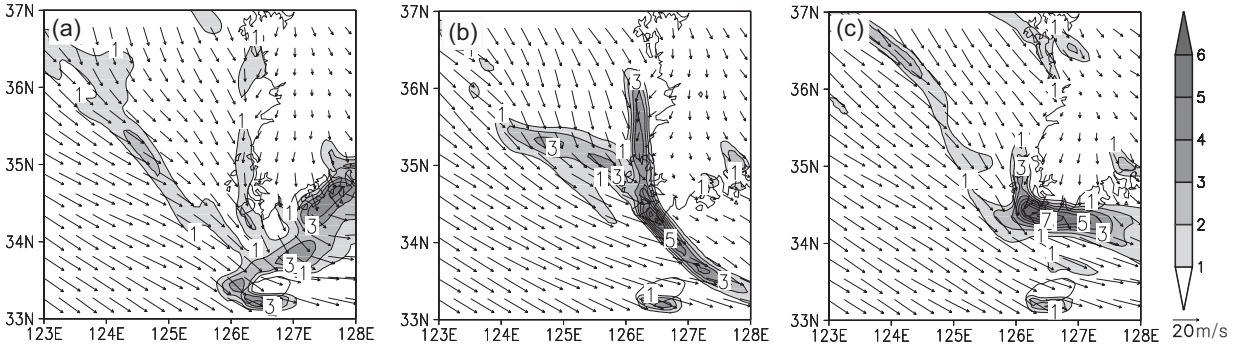

Fig. 6. The wind vector and vorticity field (10^{-4} s^{-1}) at the lowest level (50 m) from 0000 to 0600 UTC 4 December 2005 simulated by RDAPS. (a) 0000 UTC, (b) 0300 UTC and (c) 0600 UTC.

0600 UTC 4 December 2005. At 0000 UTC, a positive vorticity region is oriented NW-SE to the west of 126°E, and a NE-SW oriented high-vorticity region is seen to the east of 126°E (Fig. 6a). The positive and the high-vorticity regions correspond to the presence of shear zones formed by the difference in the northwesterly wind speed and formed by the northerly winds on the northern side and northwesterly-easterly winds on the southern side, respectively. It is also noted that a positive vorticity region is presented along the west coastal line around the longitude line 126°E with a maximum value of 3.0×10^{-4} s^{-1}. These features of the vorticity regions coincide fairly well with the C1 and C2 shown in Fig. 4a.

To investigate the characteristics of the shear zone in the initial stage, we calculate linear instability analyses according to Gill (1982, chapter 12), Ninomiya (1994) and Yanase et al. (2003). The north-south cross section of the shear zone shows that the horizontal wind shear is seen within a width of 30 km below 1000 m and its maximum magnitude reaches 5.9×10^{-4} s^{-1} near 34°N, 126°E (not shown). According to the linear barotropic instability theory, the barotropically unstable disturbance occurs only for wave numbers that are less than a cut-off value given by kL=0.639, and the maximum value for the growth rate is given by $\sigma_{\max}$=0.2012dU/dy, when kL=0.398, where $k, L, dU/dy$ are the wavenumber, half-width of the shear zone and the lateral wind shear, respectively. It is estimated that $\sigma_{\max}$ is 1.2×10^{-4} s^{-1} for the width of 30 km (L=15 km) at maximum wavelength of 236 km given by $\lambda_{\max} = 2\pi/k$, which corresponds to an e-folding time of 3.4 hours. Gill (1982, chapter 12) also explained the linear baroclinic instability. It occurs only when NkH <1.200 f, and the maximum growth rate is given by $\sigma_{\max}$=0.3098$(f/N)dU/dz$ when NkH = 0.803 f, where N, H, f and dU/dz are the Brunt-Väisällä frequency, half-depth of the layer where the disturbance exists, Coriolis parameter and the vertical shear of the geostrophic wind speed, respectively. In the present case, it is estimated that $\sigma_{\max}$ is 1.4×10^{-5} s^{-1} at the maximum wavelength of 463 km, which corresponds to an e-folding time of 10.6 hours, where $dU/dz \approx 5.2 \times 10^{-3}$ s^{-1} and $N \approx 9.7 \times 10^{-3}$ s^{-1}. This result cannot explain the rapid growth of the mesocyclone. Therefore, it is concluded that the barotropic instability is the dominant mechanism in the cyclogenesis process of the present mesocyclone.

At 0300 UTC, the positive vorticity region to the west of 126°E moves slightly eastward while being intensified, and merges with the other two vorticity regions. The maximum vorticity of 7.3×10^{-4} s^{-1} is located near (34.3°N, 126.3°E), and then, the baroclinic instability increases (Fig. 6b). At 06 UTC, it reaches the mature stage. The high-vorticity region of tilted-Y type at 0300 UTC (Fig. 6b) is concentrated near (34.2°N, 126.5°E) with the maximum vorticity of 8.3×10^{-4} s^{-1} (Fig. 6c), at this point the mesocyclone is highly developed. At this time, the above-mentioned merging of C2 with C1 can be seen.

The total surface heat flux is larger than 800–1200 W m^{-2} over the Yellow Sea while it is less than 400 W m^{-2} in the coastal region. The latent surface heat flux exceeds the sensible surface heat flux by 100–300 W m^{-2} in the Yellow Sea and the coastal region (not shown), while the sensible heat flux is generally about 1.5 times as large as the latent heat flux (Yanase et al., 2003).

To analyze the effect of the latent and sensible surface heat flux from the warm ocean, Fig. 7 shows the difference of the horizontal wind at $z = 10$ m and the increment of the latent and sensible surface heat flux between 0000 UTC and 0300 UTC 4 December 2005 (developing stage minus initial stage). An anomalous cyclonic circulation is found near (35°N, 126°E). The latent and sensible surface heat fluxes increase around the center of the anomalous cyclonic circulation and increase in the enhanced region of surface wind speed. This means that the increment of surface heat fluxes is crucially influenced by the wind. It is noted that the increment of the latent heat flux on the southern

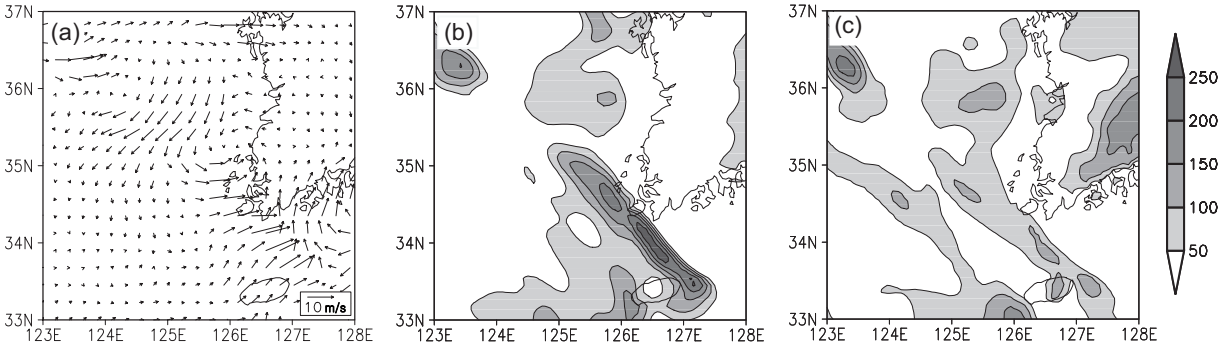

Fig. 7. (a) The difference of wind vector (z=10 m), (b) the increment of the latent surface heat flux (W m^{-2}) and (c) the increment of the sensible surface heat flux (W m^{-2}) between 0000 UTC (initial stage) and 0300 UTC 4 December 2005 (developing stage).

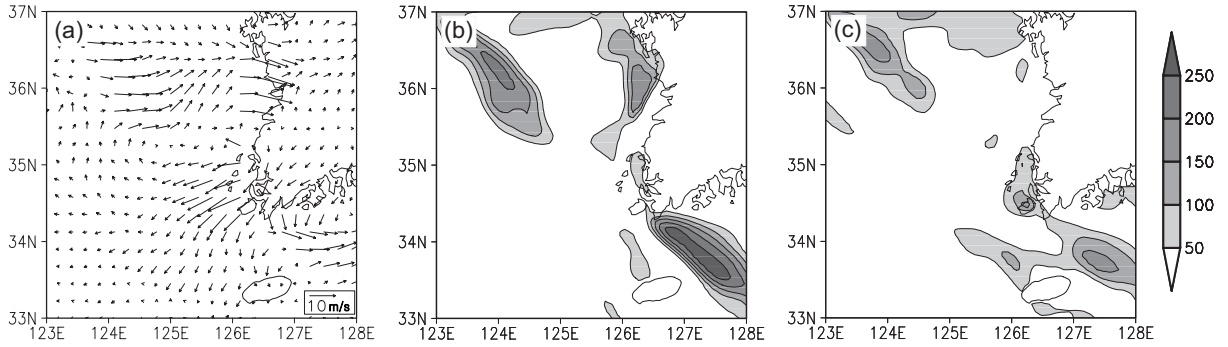

Fig. 8. Same as Fig. 7 except for between 0300 UTC (developing stage) and 0600 UTC 4 December 2005 (mature stage).

side of the anomalous cyclonic circulation exceeds 200 W m^{-2} while it is less than 100 W m^{-2} on the northern side. This asymmetric distribution is not shown in the sensible heat flux field. The enhanced cyclonic circulation corresponding to the deepening of the surface trough indicates the development of the mesocyclone, which results from the relationship between the intense surface heat fluxes and the wind. Between 0300 UTC and 0600 UTC 4 December 2005 (mature stage minus developing stage), the enhanced cyclonic circulation, which moves southward, is superimposed on the enhancement of surface heat fluxes and wind speed (Fig. 8). The enhanced region of total surface heat flux, with its increment of 400 W m^{-2} over the region of the anomalous cyclonic circulation, moves to the southeast near (33.7°N, 127.5°E). That region is also affected by the change in the latent heat flux more than the change in the sensible heat flux; this is the same as the developing stage. Therefore, it is concluded that the latent heat flux plays a more important role in the development of the mesocyclone than the sensible heat flux. The increasing wind speed corresponds to the increasing surface heat fluxes, which cause the strong low-level baroclinic instability. Consequently, the mesocyclone accompanied by the snowstorm is developed by the low-level baroclinic instability.

In order to investigate the vertical structure of the mesocyclone more in detail, Fig. 9 shows the longitude-height cross sections at 34.3°N. The latitude line 34.3°N is selected due to the location of the highest-vorticity region seen in Figs. 6b and c. The fields presented in the cross-sections are the potential temperature, vertical velocity and vorticity. In the developing stage, the vertical cross-sections of the mesocyclone shown in Figs. 9a and 9b indicate that the mesocyclone is a shallow disturbance with a "warm core" structure. The potential temperature presented a funnel-like "warm core" structure around the mesocyclone center below 700 hPa. The rising motion corresponds to this "warm core" structure which is closely related to the region of enhanced surface heating shown in Figs. 7b and 7c. The vertical cross-section of vertical velocity (w) shows that a strong rising motion is found on the eastern side of the mesocyclone center with a maximum value of 0.45 m s^{-1} at 850 hPa (Fig. 7b). It is also seen that its vorticity is mostly concentrated below 850 hPa and is largest near the surface with a maximum value of 5.5×10^{-4} s^{-1}. The maximum upward motion reaches 0.3 m s^{-1} at 750 hPa on the western side of the center, correspond-

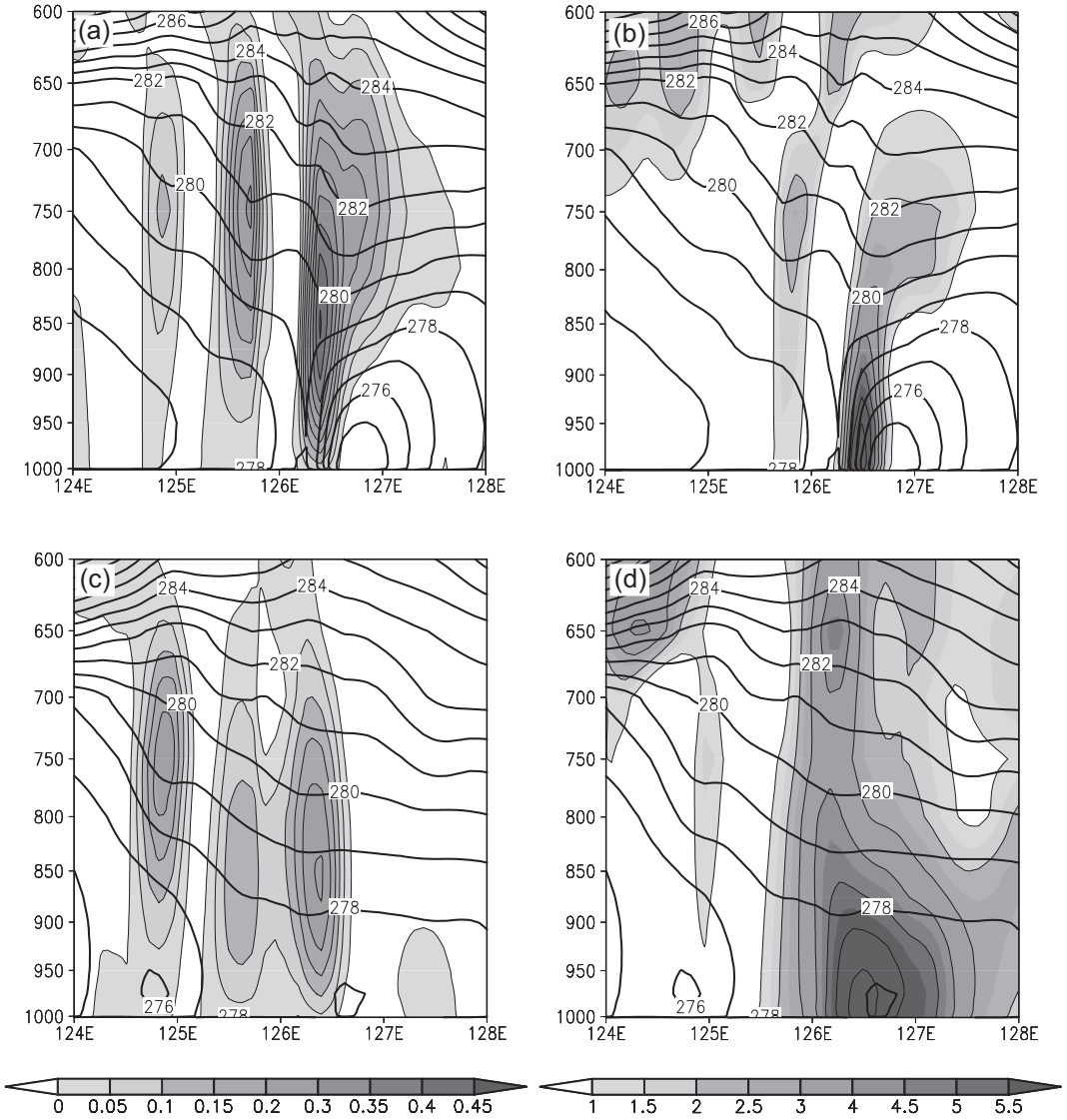

Fig. 9. The longitude-height cross-section at latitude line 34.3°N. (a) potential temperature (θ, K, contours) and vertical velocity (m s^{-1}, shaded) and (b) potential temperature (K, contours) and the vorticity (10^{-4} s^{-1}, shaded) at 0300 UTC 4 December 2005. (c) and (d) are the same as (a) and (b) except at 0600 UTC 4 December 2005, respectively.

ing to the maximum vorticity of 2.5×10^{-4} s^{-1}. It is also seen in the mature stage that both the maximum vorticity region below 850 hPa and the positive vorticity region extend eastward. The positive vorticity region extends horizontally from 125.5°E to 128.5°E and extends vertically from 700 hPa up to 500 hPa (now shown).

Figure 10 shows the longitude-height cross-sections of equivalent potential temperature, mixing ratio of total water (including cloud ice, cloud water, rain, snow, graupel), and the u-w wind vector field from 122°E to 128°E at 34.3°N. In the initial stage, the mixed layer developed up to 650 hPa and existed from 123°E to 125°E with weak convective instability while the mixed layer between 124.5°E and 125.5°E is below 800 hPa with strong convective instability and upward motion (Fig. 10a). In the developing stage, the maximum upward motion is near 126.2°E, and a cloud moves eastward and develops up to 600 hPa level. This upward motion begins at low levels and is associated with low-level surface heating. It reaches up to 550 hPa because convective instability is stronger over this region (Fig. 10b). In the mature stage, the upward motion is consistent with the convective instability near 125°–126°E, and the cloud that existed to the northwest of the mesocyclone (above-mentioned C1) extends eastward and develops due to destabilization caused by enhanced low-level surface heating and condensation

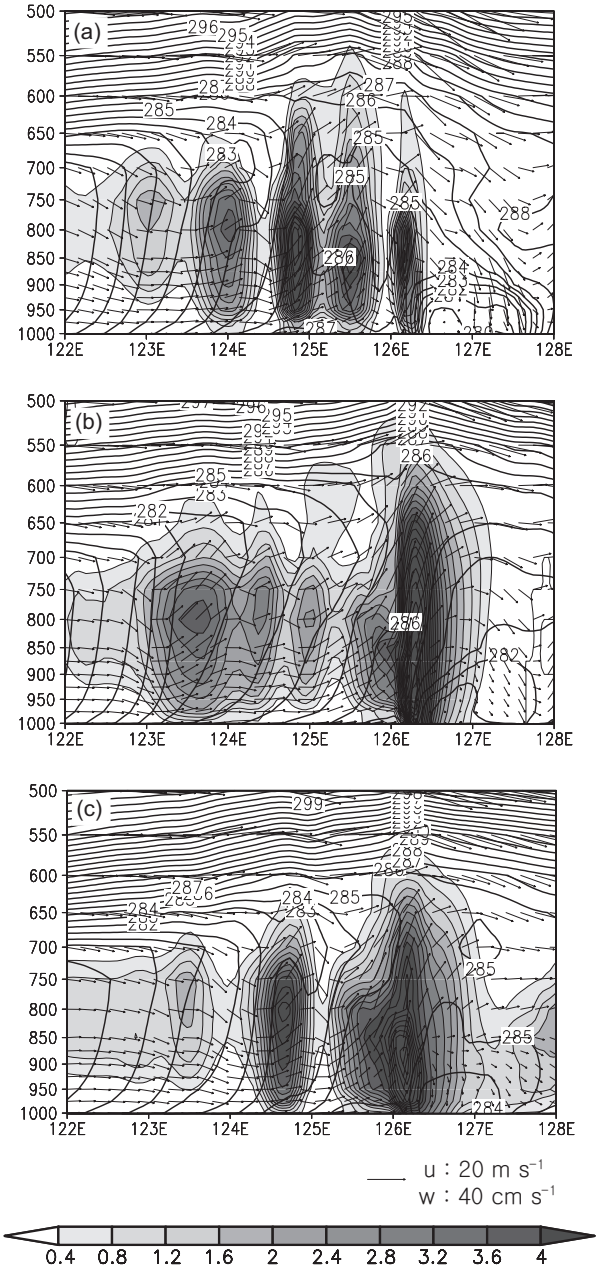

Fig. 10. The x-z cross-section (34.3°N) of equivalent potential temperature (θ_e, K, contour), mixing ratio of total water (cloud ice + cloud water + rain + snow + graupel, g kg^{-1}, shaded), and u-w wind vector at (a) 0000 UTC 4 December 2005, (b) 0300 UTC 4 December 2005 and (c) 0600 UTC 4 December 2005.

to the east of the mesocyclone center (Fig. 10c).

Figure 11 shows the temporal variation of vertically integrated moisture flux convergence (VIMFC) from 122°E to 128°E at 34.5°N. VIMFC is defined in this study as the horizontal moisture flux convergence integrated between 1000 hPa and the cloud top height of 600 hPa.

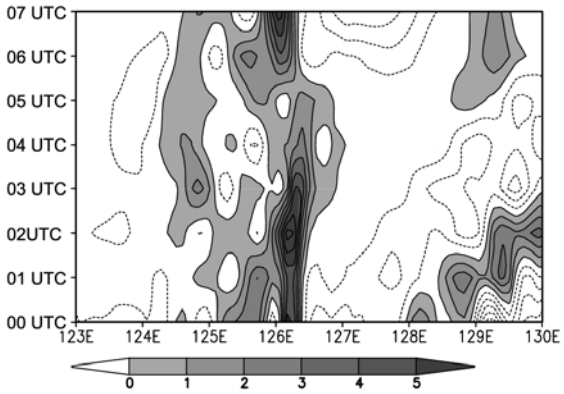

Fig. 11. Hovmöller diagram of vertically integrated moisture flux convergence (10^{-5} kg m^{-2} s^{-1}) as a function of longitude during the period from 0000 UTC 4 December 2005 to 0700 UTC 4 December 2005. Shaded area indicates the positive values.

$$\mathrm{VIMFC} = -\frac{1}{g}\int_{600\ \mathrm{hPa}}^{1000\ \mathrm{hPa}} \left(\frac{\partial uq}{\partial x} + \frac{\partial vq}{\partial y}\right) dp\,, \qquad (1)$$

where q, u and v are the specific humidity, zonal and meridional components of the wind velocity, respectively, p is the pressure and g is the acceleration due to gravity. VIMFC is calculated by the summation of the horizontal moisture flux convergence, and the units of VIMFC are 10^{-5} kg m^{-2} s^{-1}.

In initial stage, VIMFC exists near 125°–126.5°E at 0000 UTC. As the time elapsed, the region of positive VIMFC to the west of 126°E moves eastward, while that to the east of 126°E is stationary and strengthens during 0300 UTC and 0600 UTC 4 December 2005. These two regions are merged into one and intensify with a maximum value of 7×10^{-5} kg m^{-2} s^{-1} at 0200 UTC. The high-VIMFC region is also found during 0100 UTC and 0400 UTC to the east of 126°E where the heavy snow is observed 3 hours later than 0100 UTC as seen in Fig. 5. In other words, the snowstorms occurred 3 hours after the time of the maximum VIMFC. Therefore, the moisture flux convergence in advance of the snowstorm plays an important role in the formation of heavy snowfall.

The vertical profile of the data obtained from radiosonde soundings over Gwangju shows the convective mixed layer between 620 hPa and the surface at 0000 UTC 4 December 2005 (Fig. 12a). As a cold air mass moves over a warm ocean surface, a favorable environment for convection is created by an unstable lapse rate brought on by the heating and moistening in the colder air at the low-level. At 0600 UTC, the stronger capping inversion above the convective mixed layer permits a deep, moist, and well-mixed layer. Because the intensity of convection is more closely re-

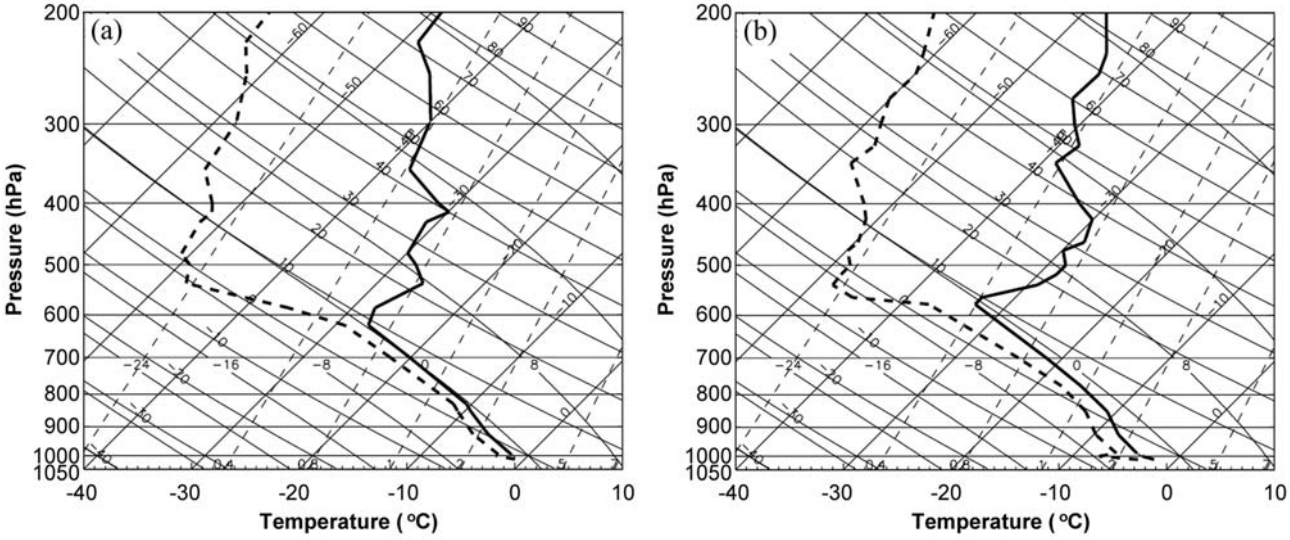

Fig. 12. Profiles of air temperature (thick solid line) and dew point (thick dashed line) obtained from radiosonde soundings over Gwangju station (35.1°N, 126.8°E) at (a) 0000 UTC and (b) 0600 UTC 4 December 2005.

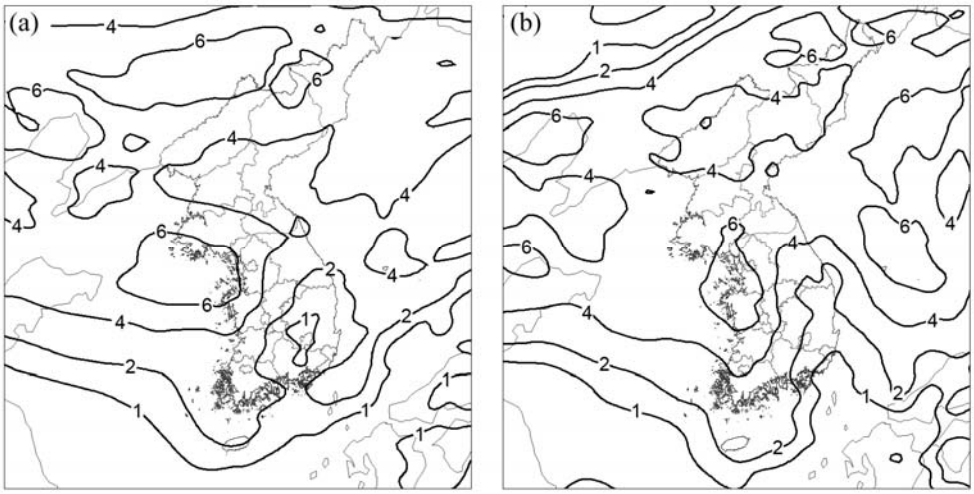

Fig. 13. Isentropic Potential vorticity on the 300 K isentropic level with a contour interval of 1 PVU at (a) 0000 UTC 4 December 2005 and (b) 0600 UTC 4 December 2005.

lated to the depth of the convective mixed layer than to the degree of lower atmospheric thermal instability (Penc, 2001), the convection grows stronger with a near-surface super adiabatic layer and a well-mixed cloud layer.

In order to investigate the evolution of the mesocyclone, we analyzed the isentropic potential vorticity (IPV). Figure 13 displays the potential vorticity (PV) on the upper-level 300 K isentropic level. PV on an isentropic level is formulated as follows.

$$\mathrm{PV}_\theta = -g(\varsigma_\theta + f)\frac{\partial\theta}{\partial p} = \frac{(\varsigma_\theta + f)}{\sigma} \qquad (2)$$

$\sigma = (-\frac{1}{g})\frac{\partial p}{\partial\theta}$ is the static stability parameter on the isentropic surface, ς and p are relative vorticity and pressure, respectively. PV is conserved on isentropic surfaces (Holton, 2004). The present case is well related to the stratospheric intrusion that developed over the Korean Peninsula. At 0000 UTC, the high PV region of 6 PVU (1 PVU=10^{-6} m^2 K s^{-1} kg^{-1}) can be seen over the Yellow Sea, and the location of the 2 PVU coincides with the approximate location of the meso-cyclogenesis (Fig. 13a). The high PV region has moved eastward over the western coast and then it attenuates and expands southward at 0600 UTC (Fig. 13b). A higher PV contour of 4 PVU is located near 35°N around the Korean Peninsula, which is related to the stratospheric intrusion. A PV descending from the lower stratosphere to the troposphere, combined

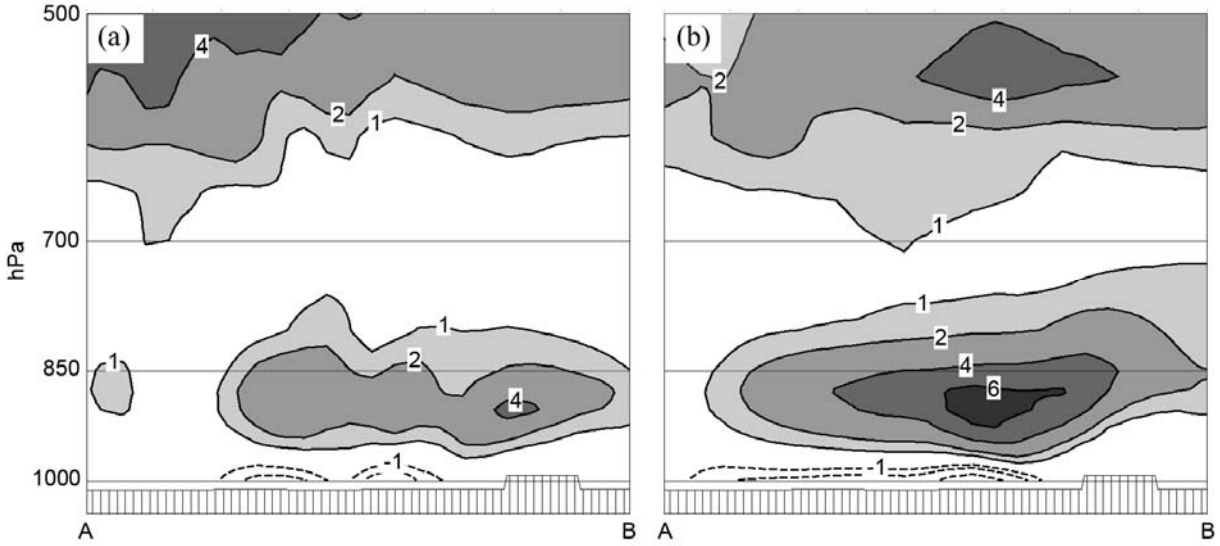

Fig. 14. Vertical cross-section of potential vorticity at (a) 0000 UTC, (b) 0600 UTC 4 December 2005 along line A–B.

with the low-level PV anomaly due to surface diabatic heating in the Yellow Sea, forms a large tropospheric PV column, which leads to unsettled weather. The PV perspective discussed in Hoskins et al. (1985) indicated that the interaction between an approaching upper-level PV anomaly and low-level baroclinicity was favored by a deep convective boundary layer. This interaction could provide the mechanism to develop cyclonic circulation for the development of the mesocyclone. To analyze the interaction, Fig. 14 shows the vertical cross-section of PV at 0000 UTC and 0600 UTC 4 December 2005 along the line AB as indicated in Fig. 1a. An upper-level PV of 1.0 PVU extends downward to 700 hPa and approaches over a low-level baroclinic zone at 0000 UTC. At 0600 UTC, the upper-level PV moves eastward to the region of enhanced low-level PV with a maximum value of 6 PVU (Fig. 14b). This low-level maximum PV is not generated in the upper-level but originates from large surface diabatic heating (Figs. 7 and 8). This low-level PV anomaly plays an important role in the formation of the mesocyclone because a cyclonic wind field is associated with a positive PV anomaly. Furthermore, the interaction between upper and lower-level PV maxima leads to an amplification of the disturbance in the mature stage of mesocyclone. Subsequently, according to Emanuel (1994), this mechanism of the interaction between upper and low-level PV anomalies produces baroclinic cyclogenesis. Thus, it is concluded that the heavy snowfall accompanying the mesocyclone results from the interaction between upper and low-level PV anomalies and the baroclinic instability due to cold air advection over a warm sea surface.

4.3 *Summary*

The evolution of the mesocyclone over the western coast is discussed in three stages. These are initial stage, developing stage and mature stage. In the initial stage of mesocyclone formation, the mesocyclone is generated by the barotropic shear instability in the horizontal shear zones where the convective cloud bands exist as relatively large cloud clusters. In the developing stage, the mesocyclone is developed by enhanced convection, anomalous cyclonic circulation, and the baroclinic instability corresponding to surface diabatic heating and moistening from the warm ocean. The increment of the latent heat flux, which is about 2 times as large as that of the sensible heat flux, exceeds 200 W m^{-2} around the anomalous cyclonic circulation. The high-VIMFC is presented 3 hours earlier than the heavy snowfall. These conditions produce a good environment for the development of convective clouds and the snowstorm itself. In the mature stage, two convective clouds, one moving eastward, the other stagnant, merge together and increase in thickness. The upward motion is increased by the convective instability around the center of the mesocyclone due to enhanced low-level surface heating and an interaction between upper and low level PV anomalies. It is found that the moisture flux convergence and the convection intensified by the development of convective mixed layer lead to the formation of the severe snowstorm.

5. Conclusion

The present study investigates the formation and evolution of a mesocyclone related to the heavy snowfall that occurred over the southwestern coast of Korea

on 4 December 2005. This mesocyclone has a synoptic environment where the dry air is advected from the continental polar air mass to the warm Yellow Sea. In satellite imagery, it is seen that two convective clouds are generated in the low-level horizontal shear zones, and mature as large convective clouds form from the merging of the two convective clouds over the western coast.

We used the mesoscale model output of RDAPS as well as surface observation, radiosonde sounding and MTSAT-1R satellite data. The evolution of the mosocyclone is discussed in three stages. In the initial stage, the cyclonic circulation is formed by the barotropic instability in the shear zone over the Yellow Sea. In the developing stage, the mesocyclone deepens over the western coast due to the enhanced convection and baroclinic instability corresponding to surface heating and moistening. In the mature stage, the mesocyclone is intensified by the destabilization caused by enhanced low-level heating and condensation, the moisture flux convergence, the interaction between upper and low level PV anomalies. These are the main causes of the strengthening of the mesocyclone.

The primary process affecting the cyclogenesis is barotropic instability according to the linear instability analysis. The baroclinic instability caused by enhanced surface heating plays an important role in the development of the mesocyclone in conjunction with the convective instability and the interaction between upper and low level PV anomalies. Also, the convection is intensified by the height of a convective mixed layer which has reached a height of 600 hPa and higher. These results suggest that the analyses of upper level IPV, low-level barotropic and baroclinic instability, VIMFC, the interaction between upper and low-level PV anomalies, and the height of convective mixed layer should be carried out to predict the mesocyclone accompanying the snowstorm.

Acknowledgements. This work was supported by a grant of "Eco-Technopia 21 Project" by Korean Ministry of Environment. This work was also supported by the Brain Korea 21 Project in 2006/7. Reviewer Prof. Gang Fu's constructive comments and suggestions are greatly appreciated. Also, we thank the Information Management Division of Korean Meteorological Administration for providing us with the Forecaster's Analysis System.

REFERENCES

Cho, I. H., H. D. Yoo, W. J. Lee, and K. S. Shin, 2004: Analyses of the heavy snowfall event occurred over the middle part of the Korean Peninsula on March 4, 2004 and suggestions for the future forecast. *Atmosphere*, **14**(3), 3–18. (in Korean with English abstract)

Dudhia, J., 1989: Numerical study of convection observed during winter monsoon experiment using a mesoscale two-dimensional model. *J. Atmos. Sci.*, **46**, 3077–3107.

Dudhia, J., 1996: A multi-layer soil temperature model for MM5. Preprints, *The Sixth PSU/NCAR Mesoscale Model Users' Workshop*, 22–24 July 1996, Boulder, Colorado, 49–50.

Emanuel, K. A., 1994: Sea-air heat transfer effects on extratropical cyclones. *Proc. Conf. on the Life Cycles of Extratropical Cyclones*, Bergen, Norway, 27 June to 1 July 1994, Amer. Meteor. Soc., 67–72.

Fu, G., H. Niino, R. Kimura, and T. Kato, 2004: A polar low over the Japan Sea on 21 January 1997. Part I: Observational analysis. *Mon. Wea. Rev.*, **132**(7), 1537–1551.

Gill, A. E., 1982: *Atmosphere-Ocean Dynamics*. Academic Press, 662pp.

Heo, K. Y., K. J. Ha, and S. H. Shin, 2005: On development mechanism of heavy snowfall event occurred in Busan on 5 March 2005. *Journal of the Korean Meteorological Society*, **41**(4), 547–556. (in Korean with English abstract)

Holton, J. R., 2004: *An Introduction to Dynamic Meteorology*. 4th ed, Elsevier Academic Press, 535pp.

Hong, S.-Y., and H.-L. Pan, 1996: Nonlocal boundary layer vertical diffusion in a medium-range forecast model. *Mon. Wea. Rev.*, **124**, 2322–2339.

Hoskins, B., M. McIntyre, and A. Robertson, 1985: On the Use and Significance of Isentropic Potential Vorticity Maps. *Quart. J. Roy. Meteor. Soc.*, **111**, 877–946.

Kain J. S., and J. M. Fritsch, 1993: Convective parameterization for mesoscale models: The Kain-Fritsch scheme. *The Representation of Cumulus Convection in Numerical Models, Meteor. Monogr.*, K. A. Emanuel and D. J. Raymond, Eds., Amer. Meteor. Soc., 165–177.

Lee, T. Y., Y. Y. Park, and Y. L. Lin, 1998: A numerical modeling study of mesoscale cyclogenesis to the east of the Korean Peninsula. *Mon. Wea. Rev.*, **126**(9), 2305–2329.

Ninomiya, K., 1994: A meso-scale low family formed over the northeastern Japan Sea in the northwestern part of a parent Polar low. *J. Meteor. Soc. Japan*, **72**(4), 589–603.

Penc, R. S., 2001: Moisture Analysis of a Type I cloud-topped boundary layer from Doppler radar and rawinsonde observations. *J. Atmos. Oceanic Technol.*, **18**(12), 1941–1958.

Reisner, J., R. J. Rasmussen, and R. T. Bruintjes, 1998: Explicit forecasting of supercooled liquid water in winter stroms using the MM5 mesoscale model. *Quart. J. Roy. Meteor. Soc.*, **124B**, 1071–1107.

Seo, E. K., and J. G. Jhun, 1991: A case study of the heavy snowfalls occurred in the Korean Peninsula from 29 January to 1 February 1990. *Journal of the Korean Meteorological Society*, **27**(2), 165–179. (in

Korean with English abstract)

Xu, Y., and M. Zhou, 1999: Numerical simulations on the explosive cyclogenesis over the kuroshio current. *Adv. Atmos. Sci.*, **16**(1), 64–76.

Yanase, W., G. Fu, H. Niino, and T. Kato, 2003: A Polar Low over the Japan Sea on 21 January 1997. Part II: A Numerical Study. *Mon. Wea. Rev.*, **132**(7), 1552–1574.

Yih, A. C., and J. E. Walsh, 1991: Sensitivities of numerical model forecasts of extreme cyclone events. *Adv. Atmos. Sci.*, **8**(1), 51–66.